Depth-variant azimuthal anisotropy in Tibet revealed by surface wave tomography

Eric Debayle, Shantanu Pandey, Xiaohui Yuan, Frederik Tilmann, Keith Priestley, Xueqing. Li

AGU PUBLICATIONS

Geophysical Research Letters

RESEARCH LETTER
10.1002/2015GL063921

Key Points:
- Surface wave tomography revealed depth-dependent azimuthal anisotropy in Tibet
- The dominant fast direction is EW at shallower depths and NS at greater depths
- The surface wave model can predict some features of *SKS* splitting measurements

Supporting Information:
- Text S1 and Figures S1–S5

Correspondence to:
X. Yuan,
yuan@gfz-potsdam.de

Citation:
Pandey, S., X. Yuan, E. Debayle, F. Tilmann, K. Priestley, and X. Li (2015), Depth-variant azimuthal anisotropy in Tibet revealed by surface wave tomography, *Geophys. Res. Lett.*, *42*, 4326–4334, doi:10.1002/2015GL063921.

Received 19 MAR 2015
Accepted 14 MAY 2015
Accepted article online 18 MAY 2015
Published online 3 JUN 2015

Depth-variant azimuthal anisotropy in Tibet revealed by surface wave tomography

Shantanu Pandey[1,2], Xiaohui Yuan[1], Eric Debayle[3], Frederik Tilmann[1,4], Keith Priestley[5], and Xueqing Li[1]

[1]Deutsches GeoForschungsZentrum GFZ, Telegrafenberg, Potsdam, Germany, [2]AWI Bremerhaven, Bremerhaven, Germany, [3]Laboratoire de Géologie de Lyon : Terre, Planètes, Environnement, CNRS UMR 5276, École Normale Supérieure de Lyon, Université de Lyon, Université Claude Bernard Lyon 1, Villeurbanne, France, [4]Freie Universität Berlin, Berlin, Germany, [5]Bullard Laboratories, University of Cambridge, Cambridge, UK

Abstract Azimuthal anisotropy derived from multimode Rayleigh wave tomography in China exhibits depth-dependent variations in Tibet, which can be explained as induced by the Cenozoic India-Eurasian collision. In west Tibet, the E-W fast polarization direction at depths $<$100 km is consistent with the accumulated shear strain in the Tibetan lithosphere, whereas the N-S fast direction at greater depths is aligned with Indian Plate motion. In northeast Tibet, depth-consistent NW-SE directions imply coupled deformation throughout the whole lithosphere, possibly also involving the underlying asthenosphere. Significant anisotropy at depths of 225 km in southeast Tibet reflects sublithospheric deformation induced by northward and eastward lithospheric subduction beneath the Himalaya and Burma, respectively. The multilayer anisotropic surface wave model can explain some features of *SKS* splitting measurements in Tibet, with differences probably attributable to the limited back azimuthal coverage of most *SKS* studies in Tibet and the limited horizontal resolution of the surface wave results.

1. Introduction

Seismic anisotropy can place direct observational constraints on lithospheric deformation and asthenospheric flow and therefore plays a pivotal role in understanding the tectonic evolution of complex regions such as the India-Eurasian collision zone. It describes the directional dependence of seismic wave speed and can be found at different depths within the Earth [*Babuška and Cara*, 1991]. Seismic anisotropy can be caused by past deformation frozen in the lithosphere or be located in the asthenosphere reflecting present-day plate motion or shearing between the lithosphere and underlying mantle. The relation between seismic anisotropy and deformation is commonly understood in terms of strain-dependent crystal alignment of anisotropic minerals, such as olivine, through lattice-preferred orientation, or by geometric alignment of isotropic rocks through shape-preferred orientation [*Long and Becker*, 2010]. The former is the dominant mechanism in the ductile lower crust as well as in the mantle where olivine is the main mineral constituent [*Zhang and Karato*, 1995]. The latter is mostly attributed to crustal fabric or texture of cracks, melts, and foliations [*Crampin and Chastin*, 2003]. The factors and conditions which can affect the presence of anisotropy may vary on various counts including mineralogy, the magnitude and history of stress and strain, temperature and pressure conditions, environmental geometry, melt, and water content [*Karato et al.*, 2008]. These factors can influence the interpretation of observed anisotropy patterns in many ways, but as many of those variables are unknown or difficult to constrain, it is generally assumed that the fast direction of mantle anisotropy aligns with the long axis of the strain ellipsoid, identical with the shearing direction for large strains [*Long and Becker*, 2010], which is the dominant pattern development over a wide range of the controlling parameters.

Seismic anisotropy in the mantle is commonly probed by shear wave splitting [*Savage*, 1999; *Long and Becker*, 2010] and surface wave analysis [*Forsyth*, 1975; *Montagner and Tanimoto*, 1991; *Trampert and Woodhouse*, 2003; *Yuan and Romanowicz*, 2010; *Debayle et al.*, 2005; *Debayle and Ricard*, 2013]. Splitting of *SKS* waves is sensitive to anisotropy beneath a seismic station with a lateral sensitivity of up to at most a few tens of kilometers, and equivalent resolution is possible with dense arrays. However, it is a measurement accumulated along the entire path from the core-mantle boundary to the surface and therefore has no inherent depth resolution. Anisotropy is thought to be strongest in the upper mantle, because lattice-preferred orientation will only develop where deformation occurs via dislocation creep,

a process that is expected to be limited to the topmost 200–300 km in most continental regions [*Karato and Wu*, 1993]. Surface waves provide global coverage of the upper mantle, including the ocean, and are sensitive to depth-dependent anisotropy but with a limited lateral resolution of a few hundred kilometers even in relatively well sampled regional tomography models. Azimuthal anisotropy can be described by a two-dimensional vector quantity. The length represents the strength of peak-to-peak anisotropy in surface wave tomography and the delay time of shear wave splitting. The direction, which represents either the fast polarization direction (for vertically propagating *SKS* waves) or the fast propagation direction (for long-period *S* waves derived from horizontally propagating surface waves), is referred to as FPD.

The continental collision between Indian and Eurasian tectonic plates has resulted in a huge amount of crustal and mantle deformation over the past 50 Ma. A large number of *SKS* splitting measurements has been obtained in and around the Tibetan plateau in the last two decades to constrain the mantle deformation and to infer the boundary of the Indian and Eurasian plates at depth. As summarized by *Zhao et al*. [2010] and *Kind and Yuan* [2010], *SKS* splitting is dominated by E-W fast directions in much of Tibet that rotate to NW-SE in northeast Tibet (see also Figure S1 in the supporting information). This orientation of the FPD seems to agree with lithospheric deformation [*León Soto et al*., 2012; *Wang et al*., 2008]. The splitting times are larger in central and east Tibet (on average 1.0–1.5 s with the largest $>$ 2.0 s) and smaller in north and west Tibet (less than 1.0 s). In southern Tibet, *SKS* splitting shows either contradictory orientations or null splitting measurements. Variations of *SKS* splitting delays were used to constrain the underthrusting fronts of the Indian and Eurasian mantle lithospheres, assuming that the anisotropy is weak in the Indian Plate [*Chen and Özalaybey*, 1998; *Huang et al*., 2000; *Zhao et al*., 2010; *Chen et al*., 2010; *Kind and Yuan*, 2010]. The presence of large *SKS* splitting in central and northeast Tibet is attributed to the heavily deformed zone between the Indian and Eurasian Plates [*Zhao et al*., 2010]. Several studies showed that the *SKS* splitting in the Indian shield has an average delay time of 1.0 s and a dominant FPD in the absolute plate motion direction, implying a significant sublithospheric contribution [*Kumar and Singh*, 2008; *Heintz et al*., 2009; *Kumar et al*., 2010; *Saikia et al*., 2010]. Other studies interpreted the *SKS* splitting variations in Tibet as caused by a change in the dip angle of the underthrusting Indian mantle lithosphere [*Sandvol et al*., 1997; *Chen et al*., 2015], suggesting that the Indian Plate is subducted subvertically in southeast Tibet. *Gao and Liu* [2009] and *Wu et al*. [2015] showed that a two-layer anisotropy model can explain the azimuthal variation in the shear wave splitting measurements in western and central Tibet.

Previous surface wave studies provided constraints on depth-dependent upper mantle anisotropy in East Asia including Tibet [*Griot et al*., 1998; *Huang et al*., 2004; *Priestley et al*., 2006]. The motivation of the present paper is to extract and discuss the azimuthal anisotropy in our recent Rayleigh surface wave tomography study [*Pandey et al*., 2014]. As the isotropic shear wave velocity anomalies were already presented in this earlier paper, we focus on azimuthal anisotropy in Tibet, where depth-variant anisotropy is the most obvious. Our anisotropic model is largely consistent with the models of *Griot et al*. [1998] and *Priestley et al*. [2006] but contains more detailed variations. Here we compare the anisotropy derived by surface waves with *SKS* splitting measurements and discuss its relationship to deformation caused by the India-Eurasian collision. Our data indicate that multiple-layer anisotropy is present beneath Tibet and should be considered in anisotropy studies.

2. Data and Methods

The data set used for the present work consists of vertical-component Rayleigh wave seismograms recorded at more than 400 stations in China and surrounding regions between 1999 and 2007 (see supporting information Figure S2 for a map of stations and teleseismic events used). The distribution of stations helped in achieving a good coverage of path density and azimuthal distribution. An anisotropic three-dimensional (3-D) upper mantle *Sv* velocity model based on this data set was derived by multimode Rayleigh wave tomography [*Pandey et al*., 2014].

The inversion proceeds in two stages [*Pandey et al*., 2014]. The first stage includes waveform fitting of each Rayleigh wave seismogram to generate a path-specific one-dimensional (1-D) model [*Debayle*, 1999]. The waveform inversion accounts for the fundamental and higher modes up to the fourth order in the period range of 50–160 s. The upper mantle is well resolved down to a depth of 400 km. The frequency range

used does not allow the recovery of crustal structure or thickness; therefore, the crust is fixed to the isotropic 3SMAC crustal model [*Nataf and Ricard*, 1995] for derivation of the path-specific models. The second stage is regionalization, in which all of the 1-D path-average models are combined to build a 3-D anisotropic model [*Debayle and Sambridge*, 2004] by carrying out two-dimensional tomographic inversions at each depth level in turn. Besides the isotropic 3-D *Sv* velocity model, a depth-dependent distribution of azimuthal anisotropy is derived.

For Rayleigh waves propagating in a medium with azimuthal anisotropy, the effect of anisotropy on *Sv* can be approximated with $\cos(2\theta)$ and $\sin(2\theta)$ terms, where θ is the azimuth along the propagation path [*Montagner and Nataf*, 1986]. Specifically, the azimuthal variation for a long-period *Sv* wave propagating horizontally with velocity V_S at a given depth z can be approximated, at each geographical point, with the following expression

$$V_s(z) = V_{s0}(z) + A_1(z)\cos(2\theta) + A_2(z)\sin(2\theta),$$

where V_{S0} is the isotropic shear wave velocity, A_1 and A_2 are two anisotropic parameters from which we extract the strength of the anisotropy by $2\sqrt{A_1^2 + A_2^2}/V_{s0}$ and the direction of fast propagation by $0.5\mathrm{atan2}(A2, A1)$ for the *Sv* wave. During the inversion, these parameters are retrieved using the continuous regionalization algorithm of *Debayle and Sambridge* [2004]. At each depth we obtain a smooth model by imposing correlations between neighboring points using a Gaussian a priori covariance function. This covariance function is defined by standard deviations controlling the amplitude of isotropic and anisotropic model perturbations separately and by a horizontal correlation length, controlling the horizontal smoothness. In our inversion we use a horizontal correlation length of 250 km and a priori standard deviations of 0.05 km s^{-1} and 0.005 km s^{-1} for the isotropic and anisotropic components, respectively. The larger a priori standard deviation for isotropic models implies comparatively much stronger damping for the anisotropic components, essentially telling the inversion to try to fit the data preferably by introducing isotropic heterogeneity. This is required to obtain reasonable amplitudes using the expected values of elastic coefficients for the upper mantle as estimated by *Estey and Douglas* [1986].

3. Resolution Tests

In *Pandey et al.* [2014] we used a variety of tests to assess the resolution of our 3-D velocity model. The tests showed that anomalies of a few hundred kilometers in the upper mantle can be well resolved nearly everywhere in the study area including Tibet. We also constructed a Voronoi diagram (see also supporting information Figure S3) from our ray coverage, using the scheme defined by *Debayle and Sambridge* [2004]. This diagram confirms that our ray coverage would be sufficient to resolve the 2θ azimuthal variation of surface waves on a 2 by 2° grid over the study area. In practice, however, the resolution of azimuthal anisotropy is also limited by the ray approximation, the horizontal smoothing imposed in the inversion, and trade-offs with lateral heterogeneities.

In order to test the effect of smoothing and ray coverage, we performed various checkerboard tests for resolving azimuthal anisotropy. We describe the results of one of these tests in Figure S4. Layered *Sv* velocity with azimuthal anisotropy is used in the input model. Two anisotropic layers at depths of 50–100 km and >150 km, respectively, are separated by an isotropic layer at depths of 100–150 km. There are no isotropic heterogeneities in any layer of the input model. In each anisotropic layer 5% azimuthal anisotropy with perpendicularly alternating FPD is assigned to 20° × 20° checkers. The three horizontal sections correspond to these three layers. Recovery of isotropic velocity perturbations is indicated in the output models, showing weak trade-offs with anisotropy (less than 0.5% in most areas), justifying the separate interpretation of the isotropic and anisotropic patterns. Anisotropy is well resolved at depths shallower than 150 km. At 125 km depth, the input model has no azimuthal anisotropy and the recovered anisotropy is an artifact that results from vertical smearing of shallower layers. We can see that this bias is small, weaker than 1% in the study area. At depths greater than 150 km, the spatial pattern of anisotropy can be reasonably recovered, although the amplitude of anisotropy is strongly reduced, roughly by a factor of 2.

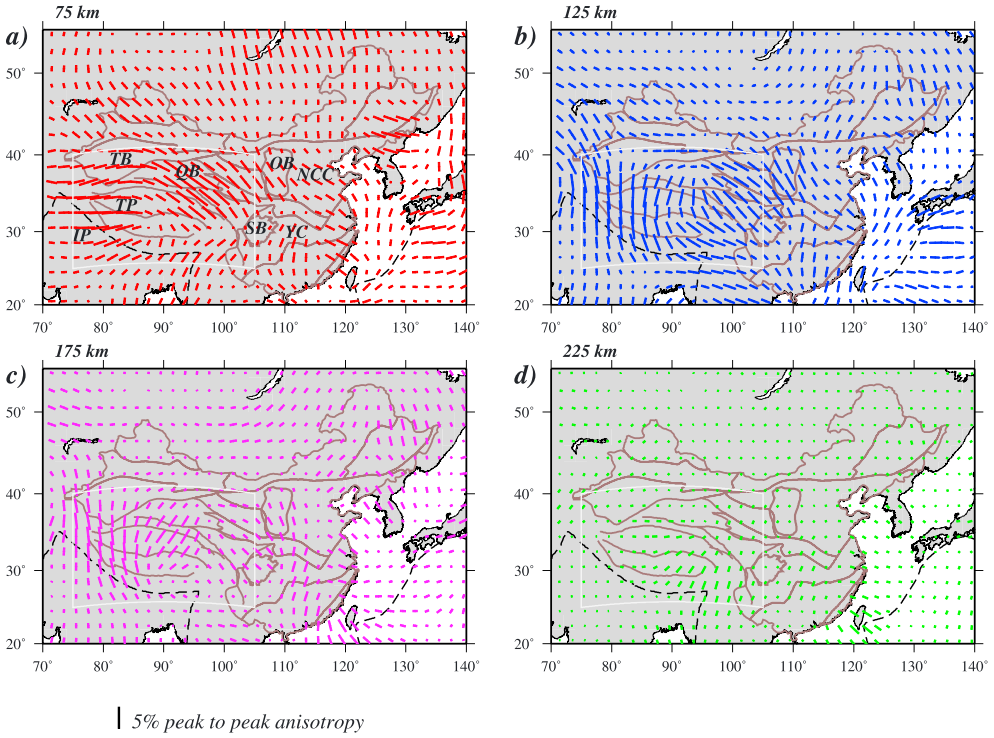

Figure 1. Maps of azimuthal anisotropy at depths of (a) 75 km, (b) 125 km, (c) 175 km, and (d) 225 km. At each depth the anisotropy is presented by horizontal bars plotted, with orientation indicating the fast direction and length scaled by the magnitude of anisotropy. The grid spacing was downsampled from 1° to 2° for map clarity. Colors indicate different depths and are consistent with those in Figure 2. Major tectonic features [from *Zhang et al*., 2011; *Pandey et al*., 2014] are marked by solid lines with main tectonic units labeled. Dashed lines indicate plate boundaries of Eurasia with Pacific/Philippine Sea and Indian plates. White box indicates the study area shown in Figure 2. Abbreviations: IP, Indian Plate; TP, Tibetan Plateau; TB, Tarim Basin; YC, Yangtze Craton; NCC, North China Craton; QB, Quaidam Basin; SB, Sichuan Basin; OB, Ordos Block.

4. Results and Interpretation

Figure 1 shows maps of azimuthal anisotropy at four different depths in and around China. The map at 75 km depth exhibits anisotropy mainly in the uppermost mantle. Because a fixed isotropic crustal model is used during the inversion, there may be some trade-off between the lowermost crust and uppermost mantle in places where the crust is thick, e.g., in Tibet. However, we do not expect that the crust will trade-off strongly with upper mantle anisotropy for three reasons. First, possible errors on isotropic crustal structure will trade-off preferentially with the upper mantle isotropic structure, owing to the much stronger damping used for anisotropic components. Second, crustal azimuthal anisotropy is expected to be weaker than crustal isotropic heterogeneities [*Babuška and Cara*, 1991], and it is reasonable to neglect its effect when using long-period (>50 s) surface waves. Third, all these effects will be limited by our excellent azimuthal coverage in the upper mantle (Figure S3). The maps at 125 and 175 km depth show anisotropy either in the lithosphere or in the asthenosphere, depending on the thickness of the lithosphere. The anisotropy at 225 km depth should mostly represent the asthenospheric flow pattern, except in the presence of steeply subducted lithosphere to the north beneath the Eastern Himalaya [*Li et al*., 2008] and to the east beneath Burma.

Strong anisotropy can be recognized at all depths in a large region involving the India-Eurasian collision zone. In this paper we concentrate on this region and highlight the depth-dependent anisotropy variations by overlaying the anisotropy at depths of 75 and 125 km (Figure 2a) and at depths of 125 and 225 km (Figure 2b). The figures show depth-dependent FPD variations in west and central Tibet and depth-consistent anisotropy in the northeastern parts of Tibet. Generally, Tibet is characterized by strong anisotropy compared to India, divided roughly by the boundary at the surface. However, whereas

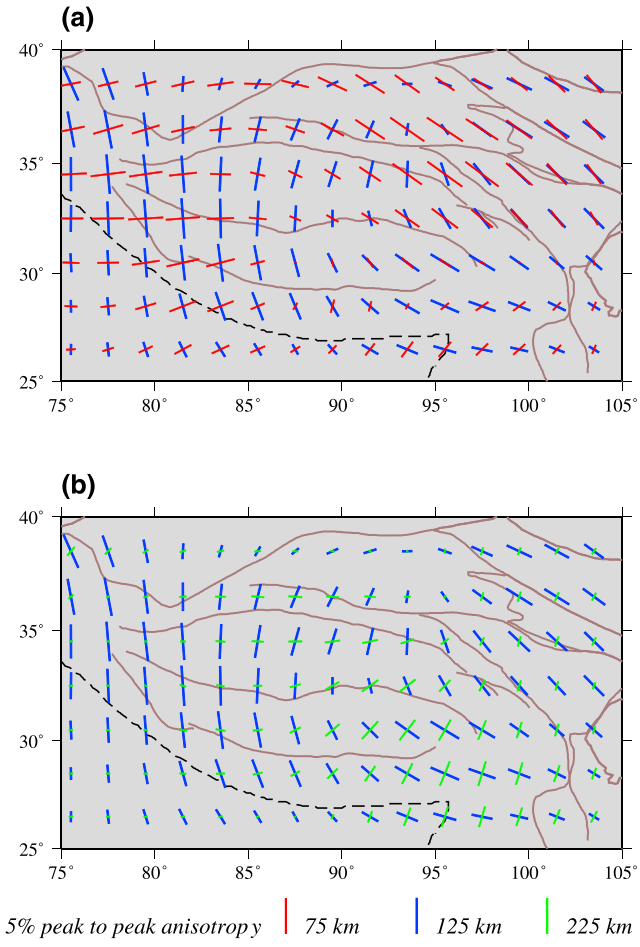

Figure 2. (a) Superposition of azimuthal anisotropy at depths of 75 km (red bars) and 125 km (blue bars). (b) Superposition of azimuthal anisotropy at depths of 125 km (blue bars) and 225 km (green bars). The zoom-in maps focus on the India-Eurasia collision zone.

this pattern is in rough agreement with previous *SKS* splitting observations, the station and event density in India is much less than in the Himalaya-Tibet area, and accordingly, the recovery of anisotropy in India in the checkerboard test (Figure S4) is much poorer.

At 75 km (Figures 1a and 2a) the FPD is dominantly E-W in west Tibet and rotates to NW-SE in northeast Tibet, and also from the Qaidam Basin to the Ordos Block crossing the northeastern margin of Tibet. The orientation of anisotropy agrees with the E-W directed shear in the crust and mantle lithosphere in reaction to Indian indentation. The anisotropy at this depth level could be seen as consistent with strain being accommodated along narrow shear zones associated with faults at the surface [e.g., *Griot et al.*, 1998]; however, the limited horizontal resolution of our data set does not allow us to resolve the degree to which strain is localized or where shear deformation is completely distributed as envisaged in the thin-sheet model, proposed in its original form by *England and McKenzie* [1982]. In addition, the FPD changes observed at 100 km depth suggest that if such a localized deformation exists, then it does not extend deeper than 100 km. Along the eastern Tibet margin (32–38°N, 98–104°E) FPDs at 75 and 125 km are subparallel, possibly reflecting outflow along a topographic gradient with stress-free basal boundary conditions [*Copley and McKenzie*, 2007], which appears to involve the mantle part of the lithosphere.

At greater depths (125 and 175 km, Figures 1b, 1c, and 2), the FPD changes to N-S direction in west Tibet, whereas it remains consistent with the shallower layer in NW-SE direction in northeast Tibet. The motion of the Indian Plate is mostly northward in a fixed hot spot reference frame (Figure 3a). In west Tibet the overall agreement of the anisotropy orientation with the Indian Plate motion thus suggests a causative link between them and is consistent with earlier studies that proposed that the Indian Plate has underthrust west Tibet all the way to the border of the Tarim Basin [*Li et al.*, 2008; *Zhao et al.*, 2010; *Kind and Yuan*, 2010]. The NW-SE orientation of the anisotropy in northeast Tibet is a feature of strong deformation of the mantle in front of the Indian Plate [*Li et al.*, 2008]. A number of seismic studies [*Li et al.*, 2008; *Chen et al.*, 2010; *Zhao et al.*, 2010; *Kind and Yuan*, 2010] suggest that the front of the northerly advancing Indian mantle lithosphere is traversing the Tibetan Plateau from northwest to southeast. North of this boundary a crush zone between two colliding plates was formed in northeast Tibet, which is characterized by low seismic velocity and strong anisotropy [*Zhao et al.*, 2010]. In particular, the softer Eurasian mantle and asthenospheric mantle displaced by the advancing Indian mantle lithosphere are pushed out to the east and south. The consistency of azimuthal anisotropy from shallow to deep layers hints at a mode of coupled deformation in the Eurasian lithosphere and underlying asthenosphere resulting from plate convergence. The GPS vectors rotate gradually from NE directed in the northeast of

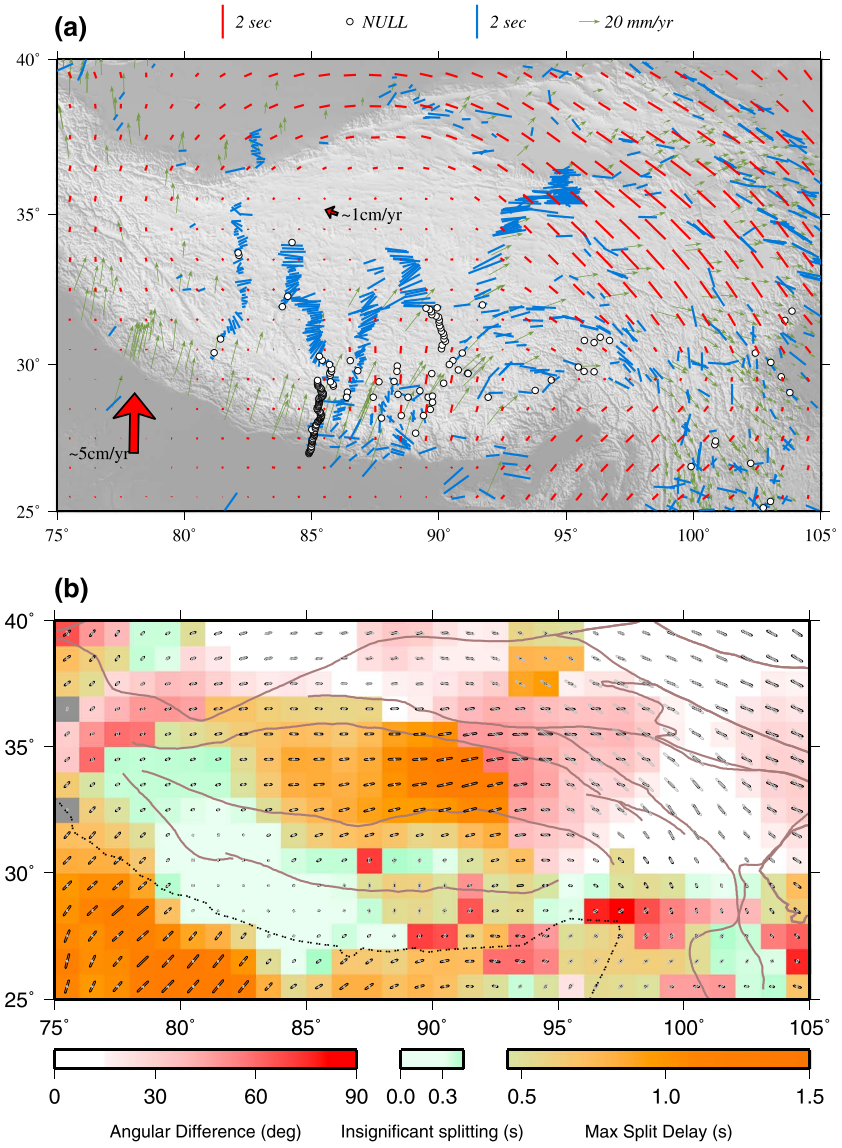

Figure 3. (a) Comparison of *SKS* splitting predicted from tomographic model (red bars) and observed *SKS* splitting (blue bars and white circles denoting null measurement) in Tibet. The length of the bars indicates splitting time delay (TD). TDs smaller than 0.3 s are considered null measurements. The *SKS* splitting data are taken from a modified version of the SplitLab database (http://splitting.gm.univ-montp2.fr/DB/public/downloadPage.php) [*Wüstefeld et al.*, 2009] and additionally from *Zhao et al.* [2010] and *Eken et al.* [2013]. Green arrows are GPS velocities with respect to stable Eurasia [*Wang et al.*, 2001]. The two red arrows denote the plate motions of the Indian and Eurasian Plates, respectively, calculated by the Plate Motion Calculator (http://www.sps.unavco.org) using the HS2-NUVEL 1A model [*Gripp and Gordon*, 1990]. (b) Differences between smoothed *SKS* measurements (plotted as black bars) and predicted splitting (gray bars, as above). White and green areas indicate regions where both anisotropy estimates agree: white for regions of significant splitting (both with TD $>$ 0.3 s) with similar fast directions less than 15° apart and green for regions where both estimates indicate no or insignificant splitting (at least one TD $<$ 0.3 s, and the other TD $<$ 0.45 s). Pink-to-red colors mark regions of significant splitting, where the fast directions disagree. Olive-to-orange marks regions where significant horizontal anisotropy is seen by one technique but not the other. The color shows the larger of observed or predicted splitting delay in this case (see supporting information for details on the calculation of the smoothed *SKS* splitting map).

the orogen (east of the Qaidam Basin) to E and SE directed along the eastern Tibetan margin with a corresponding increase in length, approximately implying extension in NW-SE direction. Taken together, these observations thus suggest consistent deformation from the upper crust into the asthenosphere. The large scale of the region of consistent NW-SE fast directions is surprising but is in line with the huge

topographic footprint of the India-Asia collision. Similar to the observations of long-period quasi-Love waves by *Chen and Park* [2013], strong anisotropy gradients are found west of the (undeformed) Yangtze Craton, suggesting a link between crustal and mantle deformation at this location, too. In southeast Tibet, the FPD has a similar NW-SE orientation and is different from that in the shallower layer (75 km). This pattern may indicate deformation within or beneath the steeply subducting Indian mantle lithosphere.

At 225 km depth, although resolution worsens, significant anisotropy, distinct from that at 175 km depth, is discernible in southeast Tibet around the Eastern Syntaxis with dominant FPD in the NE direction (Figures 1d and 2b). The anisotropy may reflect sublithospheric deformation at the northeastern edge of the Indian Plate, where it is being subducted to the north beneath the Himalaya and to the east beneath the Burma subduction zone. In this area, located at the northward tip of the Burma subduction, mantle flow might have been enhanced and aligned by this distinct subduction geometry.

5. Discussion

Multiple-layer anisotropy can explain some features of the *SKS* observations in Tibet. Following *Montagner et al*. [2000], we calculated predicted *SKS* splitting measurements by integrating the depth-dependent anisotropy from 250 km depth up to the surface and compared them with observed ones (Figure 3a). As most of the *SKS* measurements were carried out using the minimum transverse energy method of *Silver and Chan* [1991], this approach is only valid at long periods, i.e., if the splitting time is small compared to the dominant period of the *SKS* wave after filtering [*Silver and Long*, 2011]; otherwise, there is a strong back azimuthal dependence of the splitting parameters. Although the low-frequency assumption is likely to be violated in some individual cases, we nevertheless proceed with the approach of *Montagner et al*. [2000], as we lack detailed information on back azimuthal dependencies in most previous splitting results. The validness of the approach was verified by *Romanowicz and Yuan* [2012]. However, the approach of *Montagner et al*. [2000] does not account for the back azimuthal variation that would result from multiple layers of anisotropy. Although most of the *SKS* observations are station-averaged *SKS* splitting measurement [*Wüstefeld et al*., 2009], the *SKS* back azimuthal distribution for Tibet is poor, and this may contribute to a limited agreement between predicted and observed splitting.

SKS measurements are sensitive to the local structure beneath each station whereas the surface waves have a limited horizontal resolution and average the anisotropy structure over hundreds of kilometers. In order to partially mitigate the differences in resolution, we smooth the *SKS* measurements before quantifying the difference to the surface wave predictions (see Figure 3b and supporting information). However, the smoothing procedure can only be expected to represent the structural average seen by the surface waves in areas of dense measurements. In areas with sparse measurements, a few station measurements determine the properties of the *SKS* field over wide regions, such that the difference in horizontal resolution of the two techniques can still have a strong impact. The strong *SKS* splitting observed in northeast Tibet [e.g., *León Soto et al*., 2012; *Eken et al*., 2013] results from the integrated effect along the *SKS* propagation path through an anisotropic medium with little depth variation of the FPD, resulting in surface splitting predictions consistent with the observations and bolstering the case for a large-scale coherent deformation pattern. The two-layer anisotropy in west Tibet, represented by perpendicular FPDs at depths shallower and deeper than 100 km, results in partial cancelation of *SKS* splitting (depending on the thickness and anisotropy strength of each layer) and results in smaller *SKS* splitting whose directions are in some places consistent with the observations [*Zhao et al*., 2010; *Kind and Yuan*, 2010]. In south Tibet, the heterogeneous *SKS* splitting measurements as well as many null measurements [*Sandvol et al*., 1997; *Huang et al*., 2000; *Chen et al*., 2010] have been explained by distinct differences between the anisotropy of the lithospheric and sublithospheric mantle.

Although there is an overall agreement between predicted and observed *SKS* splitting beneath some parts of the Tibetan Plateau (mainly in west and northeast Tibet), some significant differences are observed, especially beneath central Tibet, where strong *SKS* splitting with a dominant E-W oriented FPD is observed, whereas the surface wave model predicts weak or absent *SKS* splitting there due to the cancelation of the splitting induced by two layers with perpendicular FPDs.

Anisotropy derived from surface wave and *SKS* wave studies does not always agree with each other [*Montagner et al*., 2000; *Becker et al*., 2012]. Different resolutions of surface and body waves can only

explain part of the discrepancy (see Figure 3b). In the case of multiple-layer anisotropy the *SKS* splitting parameters strongly depend on the azimuth of observation [*Silver and Savage*, 1994; *Silver and Long*, 2011]. Due to the global earthquake distribution pattern and/or short duration of operation of seismic experiments, many *SKS* splitting measurements are obtained with limited azimuthal coverage. For stations in Tibet, the majority of *SKS* waves is recorded from events in Fiji-Tonga. *Gao and Liu* [2009] extended the azimuthal coverage for the permanent station in Lhasa by using *SKS*, *SKKS*, and *PKS* phases and clearly showed the azimuthal dependence of splitting parameters, indicating multiple-layer anisotropy. Also, as discussed above, our simple approach of predicting *SKS* splitting does not predict the azimuthal dependence of the observed *SKS* splitting. Finally, part of the observed differences may be explained by strong crustal anisotropy, which is not accounted for by our data set.

6. Conclusion

Depth-dependent variations of azimuthal anisotropy, derived from surface wave tomography, indicate multiple-layer anisotropy in west Tibet. The E-W directed FPD in the shallow layer is consistent with localized shear along major faults in the lower crust and the uppermost mantle, a result of the continuous shortening of the lithosphere in reaction to northward indentation by the Indian Plate. In the deeper layer the FPD is aligned N-S, coinciding with the Indian Plate motion direction. In northeast Tibet strong anisotropy with constant FPD over the entire upper 200 km of the mantle is consistent with the surface strain field, implying coupled deformation of the crust and mantle lithosphere and possibly the asthenosphere in response to the Indian indenter. At asthenopheric depths, strong anisotropy is also found beneath the Eastern Syntaxis with the FPD aligned in the NE direction, indicating some relationship to deformation induced by the Burma subduction zone. The pattern of multiple-layer anisotropy predicts weak *SKS* splitting in west Tibet and strong *SKS* splitting in northeast Tibet, in agreement with previous observations. The discrepancy in central and south Tibet may be explained by a combination of crustal anisotropy not properly accounted for in the surface wave study and the azimuthal limitation of *SKS* measurements under conditions of multiple-layer anisotropy.

Acknowledgments

The work is funded by the Deutsche Forschungsgemeinschaft (grant YU 115/2). Waveform data were downloaded from the Chinese Earthquake Network Center, the IRIS, and the GEOFON data centers. We thank the operators of many temporary and permanent networks which provided useful data for this work. Some broadband stations of the TIPAGE project are used with instruments provided by the Geophysical Instrument Pool Potsdam. Rebecca Bendick provided the GPS compilation. We thank Martha Savage and an anonymous reviewer for comments that helped us to sharpen our argument and encouraged us to make the comparison with the *SKS* results more quantitative. All figures are produced with the GMT—Generic Mapping Tools.

The Editor thanks Martha Savage and an anonymous reviewer for their assistance in evaluating this paper.

References

Babuška, V., and M. Cara (1991), *Seismic Anisotropy in the Earth*, Kluwer Acad., Dordrecht, Netherlands.

Becker, T. W., S. Lebedev, and M. D. Long (2012), On the relationship between azimuthal anisotropy from shear wave splitting and surface wave tomography, *J. Geophys. Res.*, *117*, B01306, doi:10.1029/2011JB008705.

Chen, W. P., and S. Özalaybey (1998), Correlation between seismic anisotropy and Bouguer gravity anomalies in Tibet and its implications for lithospheric structures, *Geophys. J. Int.*, *135*, 93–101.

Chen, W. P., M. Martin, T. L. Tseng, R. L. Nowack, S. Hung, and B. Huang (2010), Shear-wave birefringence and current configuration of converging lithosphere under Tibet, *Earth Planet. Sci. Lett.*, *295*, 297–304.

Chen, X., and J. Park (2013), Anisotropy gradients from QL surface waves: Evidence for vertically coherent deformation in the Tibet region, *Tectonophysics*, *608*, 346–355.

Chen, Y., W. Li, X. Yuan, J. Badal, and J. Teng (2015), Geometry of the underthrusting Indian lithosphere underneath southern Tibet revealed by shear wave splitting measurement, *Earth Planet. Sci. Lett.*, *413*, 13–24, doi:10.1016/j.epsl.2014.12.041.

Copley, A., and D. McKenzie (2007), Models of crustal flow in the India-Asia collision zone, *Geophys. J. Int.*, *169*, 683–698, doi:10.1111/j.1365-246X.2007.03343.x.

Crampin, S., and S. Chastin (2003), A review of shear wave splitting in the crack-critical crust, *Geophys. J. Int.*, *155*(1), 221–240, doi:10.1046/j.1365-246X.2003.02037.x.

Debayle, E. (1999), SV-wave azimuthal anisotropy in the Australian upper mantle: Preliminary results from automated Rayleigh waveform inversion, *Geophys. J. Int.*, *137*(3), 747–754, doi:10.1046/j.1365-246x.1999.00832.x.

Debayle, E., and M. Sambridge (2004), Inversion of massive surface wave data sets: Model construction and resolution assessment, *J. Geophys. Res.*, *109*, doi:10.1029/2003JB002652.

Debayle, E., and Y. Ricard (2013), Seismic observations of large-scale deformation at the bottom of fast-moving plates, *Earth Planet. Sci. Lett.*, *376*, 165–177.

Debayle, E., B. Kennett, and K. Priestley (2005), Global azimuthal seismic anisotropy and the unique plate-motion deformation of Australia, *Nature*, *433*, 509–512.

Eken, T., F. Tilmann, J. Mechie, W. Zhao, R. Kind, H. Su, G. Xue, and M. Karplus (2013), Seismic anisotropy from SKS splitting beneath northeastern Tibet, *Bull. Seismol. Soc. Am.*, *103*, 3362–3371, doi:10.1785/0120130054.

England, P. C., and D. P. McKenzie (1982), A thin viscous sheet model for continental deformation, *Geophys. J. R. Astron. Soc.*, *70*, 295–321.

Estey, L. H., and B. J. Douglas (1986), Upper mantle anisotropy: A preliminary model, *J. Geophys. Res.*, *91*(B11), 11,393–11,406, doi:10.1029/JB091iB11p11393.

Forsyth, D. W. (1975), The early structural evolution and anisotropy of the oceanic upper mantle, *Geophys. J. Int.*, *43*(1), 103–162, doi:10.1111/j.1365-246X.1975.tb00630.x.

Gao, S. S., and K. H. Liu (2009), Significant seismic anisotropy beneath the southern Lhasa Terrane, Tibetan Plateau, *Geochem. Geophys. Geosyst.*, *10*, Q02008, doi:10.1029/2008GC002227.

Griot, D.-A., J.-P. Montagner, and P. Tapponnier (1998), Confrontation of mantle seismic anisotropy with two extreme models of strain, in Central Asia, *Geophys. Res. Lett.*, *27*, 1447–1450, doi:10.1029/98GL00991.
Gripp, A. E., and R. G. Gordon (1990), Current plate velocities relative to the hotspots incorporating the Nuvel-1A global plate motion model, *Geophys. Res. Lett.*, *17*, 1109–1112.
Heintz, M., V. P. Kumar, V. K. Gaur, K. Priestly, S. S. Rai, and K. S. Prakasam (2009), Anisotropy of the Indian continental lithospheric mantle, *Geophys. J. Int.*, *179*, 1341–1360.
Huang, W. C., et al. (2000), Seismic polarization anisotropy beneath the central Tibetan Plateau, *J. Geophys. Res.*, *105*, 27,979–27,989, doi:10.1029/2000JB900339.
Huang, Z., Y. Peng, Y. Luo, Y. Zheng, and W. Su (2004), Azimuthal anisotropy of Rayleigh waves in East Asia, *Geophys. Res. Lett.*, *31*, L15617, doi:10.1029/2004GL020399.
Karato, S.-I., and P. Wu (1993), Rheology of the upper mantle: A synthesis, *Science*, *260*, 771–778.
Karato, S.-I., H.-Y. Jung, I. Katayama, and P. Skemer (2008), Geodynamic significance of seismic anisotropy of the upper mantle: New insights from laboratory studies, *Annu. Rev. Earth Planet. Sci.*, *36*, 59–95.
Kind, R., and X. Yuan (2010), Seismic images of the biggest crash on Earth, *Science*, *329*(5998), 1479–80, doi:10.1126/science.1191620.
Kumar, M. R., and A. Singh (2008), Evidence for plate motion related strain in the Indian shield from shear wave splitting measurements, *J. Geophys. Res.*, *113*, B08306, doi:10.1029/2007JB005128.
Kumar, N., M. R. Kumar, A. Singh, P. S. Raju, and N. P. Rao (2010), Shear wave anisotropy of the Godavari rift in the south Indian shield: Rift signature of APM related strain?, *Phys. Earth Planet. Int.*, *181*, 82–87.
León Soto, G., E. Sandvol, J. F. Ni, L. Flesch, T. M. Hearn, F. Tilmann, J. Chen, and L. D. Brown (2012), Significant and vertically coherent seismic anisotropy beneath eastern Tibet, *J. Geophys. Res.*, *117*, B05201, doi:10.1029/2011JB008919.
Li, C., R. D. van der Hilst, A. S. Meltzer, and E. R. Engdahl (2008), Subduction of the Indian lithosphere beneath the Tibetan Plateau and Burma, *Earth Planet. Sci. Lett.*, *274*, 157–168.
Long, M. D., and T. W. Becker (2010), Mantle dynamics and seismic anisotropy, *Earth Planet. Sci. Lett.*, *297*, 341–354.
Montagner, J. P., and T. Tanimoto (1991), Global upper mantle tomography of seismic velocities and anisotropies, *J. Geophys. Res.*, *96*(B12), 20,337–20,351, doi:10.1029/91JB01890.
Montagner, J.-P., and H.-C. Nataf (1986), A simple method for inverting the azimuthal anisotropy of surface waves, *J. Geophys. Res.*, *91*(B1), 511–520, doi:10.1029/JB091iB01p00511.
Montagner, J.-P., D.-A. Griot-Pommera, and J. Lavé (2000), How to relate body wave and surface wave anisotropy?, *J. Geophys. Res.*, *105*(B8), 19,015–19,027, doi:10.1029/2000JB900015.
Nataf, H. C., and Y. Ricard (1995), 3SMAC: An a priori tomographic model of the upper mantle based on geophysical modeling, *Phys. Earth Planet. Inter.*, *1–2*, 101–122.
Pandey, S., X. Yuan, E. Debayle, K. Priestley, R. Kind, F. Tilmann, and X. Li (2014), A 3D shear-wave velocity model of the upper mantle beneath China and the surrounding areas, *Tectonophysics*, *633*, 193–210, doi:10.1016/j.tecto.2014.07.011.
Priestley, K., E. Debayle, D. McKenzie, and S. Pilidou (2006), Upper mantle structure of eastern Asia from multi-mode surface waveform tomography, *J. Geophys. Res.*, *111*, B10304, doi:10.1029/2005JB004082.
Romanowicz, B., and H. Yuan (2012), On the interpretation of SKS splitting measurements in the presence of several layers of anisotropy, *Geophys. J. Int.*, *188*, 1129–1140, doi:10.1111/j.1365-246X.2011.05301.x.
Saikia, D., M. R. Kumar, A. Singh, G. Mohan, and R. S. Dattatrayam (2010), Seismic anisotropy beneath the Indian continent from splitting of direct S waves, *J. Geophys. Res.*, *115*, B12315, doi:10.1029/2009JB007009.
Sandvol, E., J. Ni, R. Kind, and W. Zhao (1997), Seismic anisotropy beneath the southern Himalayas-Tibet collision zone, *J. Geophys. Res.*, *102*(B8), 17,813–17,823, doi:10.1029/97JB01424.
Savage, M. K. (1999), Seismic anisotropy and mantle deformation: What have we learned from shear wave splitting?, *Rev. Geophys.*, *37*(1), 65, doi:10.1029/98RG02075.
Silver, P. G., and W. W. Chan (1991), Shear wave splitting and subcontinental mantle deformation, *J. Geophys. Res.*, *96*, 16,429–16,454, doi:10.1029/91JB00899.
Silver, P. G., and M. D. Long (2011), The non-commutativity of shear wave splitting operators at low frequencies and implications for anisotropy tomography, *Geophys. J. Int.*, *184*, 1415–1427, doi:10.1111/j.1365-246X.2010.04927.x.
Silver, P. G., and M. Savage (1994), The interpretation of shear-wave splitting parameters in the presence of two anisotropic layers, *Geophys J. Int.*, *119*, 949–963, doi:10.1111/j.1365-246X.1994.tb04027.x.
Trampert, J., and J. H. Woodhouse (2003), Global anisotropic phase velocity maps for fundamental mode surface waves between 40 and 150 s, *Geophys. J. Int.*, *154*(1), 154–165, doi:10.1046/j.1365-246X.2003.01952.x.
Wang, C.-Y., L. M. Flesch, P. G. Silver, and L. J. Chang (2008), Evidence for mechanically coupled lithosphere in central Asia and resulting implications, *Geology*, *36*, 363–366, doi:10.1130/G24450A.1.
Wang, Q., et al. (2001), Present-day crustal deformation in China constrained by global positioning system measurements, *Science*, *294*(5542), 574–577.
Wu, J., Z. Zhang, F. Kong, B. B. Yang, Y. Yu, K. H. Liu, and S. S. Gao (2015), Complex seismic anisotropy beneath western Tibet and its geodynamic implications, *Earth Planet. Sci. Lett.*, *413*, 167–175, doi:10.1016/j.epsl.2015.01.002.
Wüstefeld, A., G. H. R. Bokelmann, G. Barruol, and J. P. Montagner (2009), Identifying global seismic anisotropy patterns by correlating shear-wave splitting and surface waves data, *Phys. Earth Planet. Int.*, *176*, 198–212, doi:10.1016/j.pepi.2009.05.006.
Yuan, H., and B. Romanowicz (2010), Depth dependent azimuthal anisotropy in the western US upper mantle, *Earth Planet. Sci. Lett.*, *300*, 385–394.
Zhang, S., and S. Karato (1995), Lattice preferred orientation of olivine aggregates deformed in simple shear, *Nature*, *375*, 774–777.
Zhang, Z., L. Yang, J. Teng, and J. Badal (2011), An overview of the Earth crust under China, *Earth Sci. Rev.*, *104*, 143–166.
Zhao, J., et al. (2010), The boundary between the Indian and Asian tectonic plates below Tibet, *Proc. Natl. Acad. Sci. U.S.A.*, *107*(25), 11,229–11,233, doi:10.1073/pnas.1001921107.